

1 Article

2 Hydrodeoxygenation (HDO) of aliphatic oxygenates 3 and phenol over NiMo/MgAl₂O₄: Reactivity, 4 inhibition, and catalyst reactivation

5 Trine Marie Hartmann Dabros^{1,a}, Mads Lysgaard Andersen¹, Simon Brædder Lindahl¹, Thomas
6 Willum Hansen², Martin Høj¹, Jostein Gabrielsen³, Jan-Dierk Grunwaldt^{4,5} and Anker Degn
7 Jensen^{1,*}

8

9 ¹ Department of Chemical and Biochemical Engineering, Technical University of Denmark (DTU), Søtofts
10 Plads, Building 229, DK-2800 Kgs. Lyngby, Denmark; trar@topsoe.com (T.M.H.A);
11 s144152@student.dtu.dk (M.L.A); s144156@student.dtu.dk (S.B.L.); mh@kt.dtu.dk (M.H.); aj@kt.dtu.dk
12 (A.D.J.)

13 ² National Centre for Nano Fabrication and Characterization (DTU Nanolab), Technical University of
14 Denmark (DTU), Fysikvej - Building 307,
15 DK-2800 Kgs. Lyngby, Denmark; tw@cen.dtu.dk (T.W.H)

16 ³ Haldor Topsøe A/S, Haldor Topsøes Allé 1, DK-2800 Kgs. Lyngby, Denmark; joga@topsoe.com (J.G.)

17 ⁴ Institute of Catalysis Research and Technology, Karlsruhe Institute of Technology (KIT),
18 Engesserstraße 18/20, Karlsruhe, D-76131, Germany; grunwaldt@kit.edu (J.-D.G.)

19 ⁵ Institute of Catalysis Research and Technology, Karlsruhe Institute of Technology (KIT), Hermann-von-
20 Helmholtz Platz 1, Eggenstein-Leopoldshafen, D-76344, Germany; grunwaldt@kit.edu (J.-D.G.)

21 * Correspondence: aj@kt.dtu.dk; Tel.: 0045-45-25-28-41

22 ^a Current affiliation: Haldor Topsøe A/S, Haldor Topsøes Allé 1, DK-2800 Kgs. Lyngby, Denmark;
23 trar@topsoe.com (T.M.H.A)

24 Received: date; Accepted: date; Published: date

25 **Abstract:** This study provides new insights into sustainable fuel production by upgrading of bio-
26 derived oxygenates by catalytic hydrodeoxygenation (HDO). HDO of ethylene glycol (EG),
27 cyclohexanol (Cyc), acetic acid (AcOH), and phenol (Phe) was investigated using a Ni-
28 MoS₂/MgAl₂O₄ catalyst. In addition, HDO of a mixture of Phe/EG and Cyc/EG was studied as a first
29 step towards the complex mixture in biomass pyrolysis vapor and bio-oil. Activity tests were
30 performed in a fixed bed reactor at 380-450 °C, 27 bar H₂, 550 vol ppm H₂S, and up to 220 h on
31 stream. Acetic acid plugged the reactor inlet by carbon deposition within 2 h on stream, underlining
32 the challenges of upgrading highly reactive oxygenates. For ethylene glycol and cyclohexanol,
33 steady state conversion was obtained in the temperature range of 380-415 °C. The HDO macro-
34 kinetics were assessed in terms of consecutive dehydration and hydrogenation reactions. The results
35 indicate that HDO of ethylene glycol and cyclohexanol involve different active sites. There was no
36 significant influence from phenol or cyclohexanol on the rate of ethylene glycol HDO. However, a
37 pronounced inhibiting effect from ethylene glycol on the HDO of cyclohexanol was observed.
38 Catalyst deactivation by carbon deposition could be mitigated by oxidation and resulfidation. The
39 results presented here demonstrate the need to address differences in oxygenate reactivity when
40 upgrading vapors or oils derived from pyrolysis of biomass.

41 **Keywords:** Hydrodeoxygenation (HDO); ethylene glycol; acetic acid; cyclohexanol; phenol;
42 molybdenum sulfides; biomass

43

44

45 1. Introduction

46 Fast pyrolysis is a well-known method for converting solid, lignocellulosic biomass such as
47 wood and straw into bio-oil, a potential liquid hydrocarbon fuel [1]. Different catalytic processes can
48 be coupled with fast pyrolysis in order to improve particularly the heating value and the stability of
49 bio-oil. Such catalytic upgrading can be integrated in the pyrolysis step as in catalytic fast pyrolysis
50 or catalytic fast hydrolysis [2–4], and/or downstream as catalytic hydrodeoxygenation (HDO)
51 [5,6]. This downstream hydroprocessing can be performed either on pyrolysis oil vapors or on the
52 condensed bio-oil.

53 Several HDO studies on various model compounds, in particular phenolic ones, have shown
54 that a broad range of catalysts can be used for bio-oil HDO. An overview of these studies can be
55 found in recent review articles [5–7]. In real biomass pyrolysis vapors and condensed bio-oil,
56 aromatic and aliphatic compounds co-exist, exhibiting many different oxygen functionalities such as
57 alcohol, aldehyde, ketone, ester, carboxylic acid groups or furans and phenols [8–10]. The reactivity,
58 and hence also the instability, of these functionalities has been mapped out in various studies
59 [5,11,12], indicating that the most reactive bio-oil constituents originate from the cellulosic part of
60 biomass.

61 In a next step, it is particularly relevant to study the HDO of both cellulose and lignin derived
62 model compounds to understand the competitive reactions occurring during HDO of real feedstocks.
63 Dwiatmoko et al. [13] have shown that the HDO of guaiacol over a Ru/C catalyst in a batch autoclave
64 at 270 °C was strongly suppressed by the presence of furfural, when the molar furfural/guaiacol ratio
65 was increased above 0.47. This was explained by competitive adsorption, which was also observed
66 for 5-hydroxymethylfurfural. Ryymin et al. [14] reported competitive adsorption of methyl
67 heptanoate and phenol over a sulfided NiMo/Al₂O₃ catalyst operated at 250 °C in a batch reactor.
68 Boscagli et al. [15] performed HDO of phenol and D-glucose in a batch autoclave at 340 °C over
69 supported Ni and Ru catalysts. D-glucose was readily converted in water and in bio-oil. Phenol
70 conversion, however, was strongly suppressed in bio-oil. Their results show that not only the activity,
71 but also the selectivity to reaction products depended on the reaction medium. To investigate such
72 interactions further, studies are required that are conducted in continuous flow and step by step
73 allowing to process more complex reaction mixtures.

74 In this work, a sulfided NiMo catalyst with MgAl₂O₄ as water and sulfur tolerant support was
75 used to study the HDO of cellulose and lignin type model compounds in a continuous flow, fixed
76 bed reactor (EG: ethylene glycol, Cyc: cyclohexanol, Phe: phenol, and AcOH: acetic acid). Water
77 tolerance is important, since oxygen is removed as water in HDO. Deoxygenation can alternatively
78 also occur by other reactions such as decarbonylation or decarboxylation. Sulfur tolerance is
79 important, as biomass contains sulfur [16,17], which is a known poison to transition metal based
80 catalysts. Macro-kinetic models were derived to quantify the reactivity and selectivity of the
81 conversion of the C₂ and C₆ alcohols. The results show the importance of studying more complex
82 reaction mixtures during HDO of oxygenated species when upgrading vapors or oils derived from
83 fast pyrolysis of biomass.

84 2. Results

85 2.1. Reaction Thermodynamics

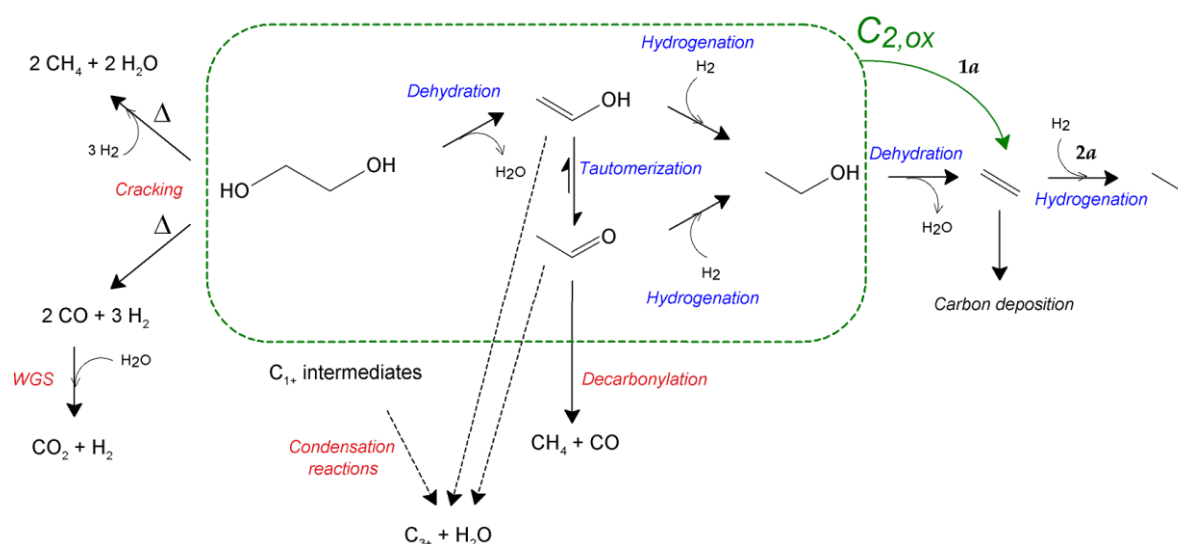
86 HDO reactions are typically exothermic, with a significant contribution from hydrogenation
87 reactions. This is also the case for the HDO of phenol into cyclohexane ($\Delta H = -290$ kJ/mol at 380–450
88 °C), of ethylene glycol into ethane ($\Delta H = -190$ kJ/mol at 380–450 °C), and of cyclohexanol into
89 cyclohexane ($\Delta H = -84$ kJ/mol at 380–450 °C), calculated with HSC Chemistry v. 9.4.1. The theoretical
90 adiabatic temperature rise that would occur from these reactions in the given experiments would be
91 165–195 °C from ethylene glycol HDO (Phe/EG, EG), 45 °C from phenol HDO (Phe/EG), and 15–50 °C
92 from cyclohexanol HDO (Cyc/EG, Cyc). The reactor temperature did in fact increase rapidly (by up
93 to 16 °C) when the liquid feed was started (Figure S3). The temperature could however be controlled,

94 as the reactor was not operated adiabatically, and to some extent also due to deactivation and
 95 occurrence of endothermic reactions, such as cracking.

96
 97
 98
 99

2.2. Reaction Schemes

100 Based on the experimental results for conversion of ethylene glycol over sulfided catalysts, the
 101 HDO reaction pathway for ethylene glycol has been assumed to consist of a series of consecutive
 102 dehydration and hydrogenation reactions (Scheme 1). Acetaldehyde is expected to form via the
 103 tautomerization of ethenol (vinyl alcohol), and both compounds can be hydrogenated to form
 104 ethanol. In other experiments, where an extended gas analysis was performed, acetaldehyde was
 105 detected in the product gas from ethylene glycol HDO over sulfided catalysts. CO and CH₄ can form
 106 from the decarbonylation of acetaldehyde, but cracking of ethylene glycol also occurred, giving a
 107 yield ratio of CO/CH₄ > 1. CO₂ can form from the water gas shift (WGS) reaction. The MgAl₂O₄
 108 support catalyzes dehydration and alcohol condensation reactions [18].
 109
 110

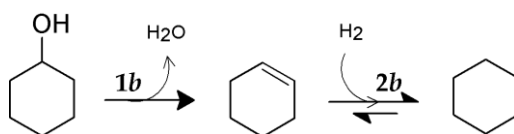


111
 112
 113
 114
 115

Scheme 1. Different reaction paths for the conversion of ethylene glycol into various C₁, C₂, and C₃₊ products; in blue: target reactions and in red: side reactions. Δ indicates additional heat. C_{2,ox} is used as a lumped term for ethylene glycol, ethenol, acetaldehyde, and ethanol. Reactions 1a and 2a are included in the macro-kinetic model, see section 4.5.

116
 117
 118
 119
 120
 121

Based on the results from the activity tests, the conversion of cyclohexanol was assumed to follow a dehydration step forming cyclohexene, which could then be hydrogenated to cyclohexane (Scheme 2). Dehydrogenation into benzene was not observed, although it is thermodynamically favorable.



122
 123
 124
 125

Scheme 2. Possible reactions of cyclohexanol HDO. ΔH = 41 kJ/mol (reaction 1b) and -124 kJ/mol (reaction 2b) at 380-450 °C. Reactions 1b and 2b are included in the macro-kinetic model, see section 4.5.

126

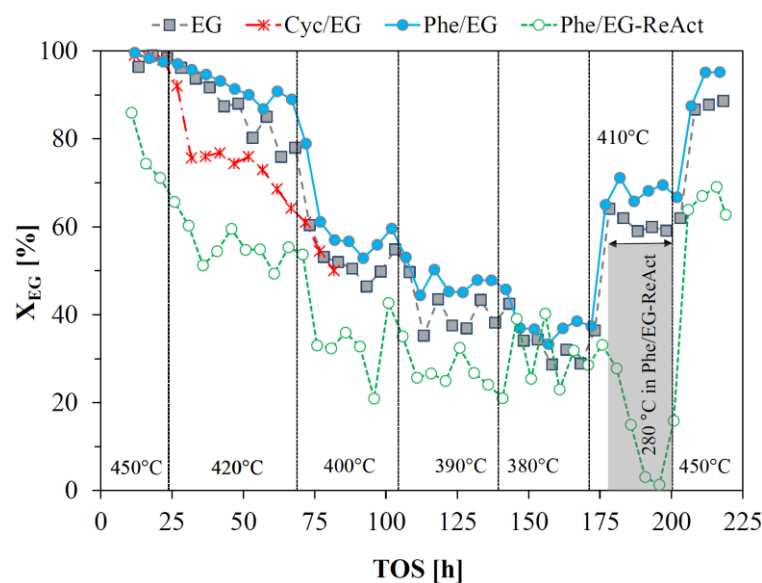
127 2.3. HDO of Ethylene Glycol

128 HDO of pure ethylene glycol and mixtures of phenol/ethylene glycol and cyclohexanol/ethylene
 129 (EG, Phe/EG, Cyc/EG) and that of the phenol/ethylene glycol mixture after catalyst reactivation
 130 (Phe/EG-ReAct, see Section 2.4) was performed in a continuous flow, fixed bed reactor at 40 barg and
 131 380 to 450 °C (see section 4). The conversion of ethylene glycol (Figure 1) was close to 100 % at 450 °C
 132 in the beginning of each experiment, except for the reactivated catalyst, where it was 86 %.
 133 Deactivation however occurred, and a decrease in conversion was observed before the temperature
 134 was decreased to 420 °C (at time on stream (TOS) = 24 h). Steady state activity was obtained at the
 135 subsequent temperature set points of 400, 390, and 380 °C. Increasing the temperature from 380 °C to
 136 410 °C after 170 h (EG and Phe/EG), did not allow for steady state operation in terms of product
 137 yields, and continuous deactivation was observed (Figure 2). As the temperature was brought back
 138 to the initial set point of 450 °C, the conversion increased to 88-95 %. It was thus slightly lower than
 139 the initially obtained conversion and continued deactivation was evident from the product yields
 140 (Figure 2).

141 The reaction temperature was identical (within <2 °C) for the experiments with pure ethylene
 142 glycol and the Phe/EG mixture. The temperature was however notably lower (up to 10 °C) when
 143 cyclohexanol was present in the feed, which affected the conversion and yields accordingly. This
 144 lower temperature was due to the endothermic dehydration of cyclohexanol.

145

146



147

148 **Figure 1.** Conversion of ethylene glycol, X_{EG} , from experiments with pure ethylene glycol and
 149 mixtures of cyclohexanol/EG and phenol/EG, and with the phenol/EG mixture after catalyst
 150 reactivation (Phe/EG-ReAct, see Section 2.4). For experimental conditions, see Materials and Methods
 151 section 4.4, Table 6. Set point temperatures are shown. For Phe/EG-ReAct, the step at 390 °C was
 152 extended by 15 h (not indicated in the figure for simplicity), until a step at 280 °C was introduced.

153

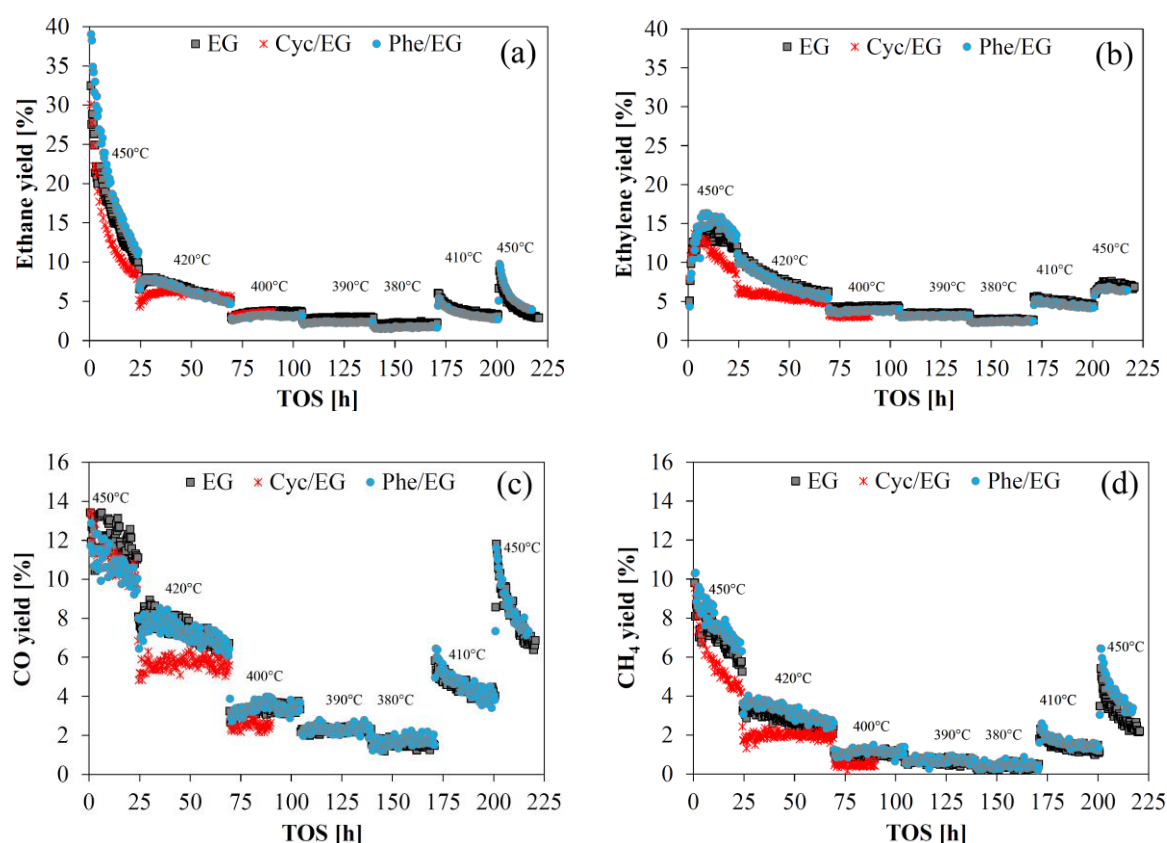
154 Figure 2 shows the yields of C₁-C₂ gas products. The yield of CO₂ was ≈ 1-5 % during the initial
 155 deactivation period and <0.5 % at the subsequent steady states. There was an initial (TOS < 10 h)
 156 decrease in the yield of ethane and a corresponding increase in ethylene (Figure 2a-b). This initial
 157 deactivation in hydrogenation activity was presumably caused by loss of SH-groups from the active
 158 edges of the promoted MoS₂ particles [19], while carbon deposition also contributed to the overall

159 deactivation. During steady state operation at 380-400 °C, the yields of ethane and ethylene,
 160 respectively, were below 5 %. The yields obtained immediately after returning to 450 °C at 200 h were
 161 approximately the same as obtained at 24 h, at the end of the initial 450 °C operation period,
 162 supporting the observation that steady state activity was obtained during 70-170 h on stream with
 163 little further deactivation during this period.

164 CO was the main cracking product formed (Figure 2c-d). The C_2/C_1 yield ratio obtained in the
 165 experiments (Figure 3) increased linearly with decreasing temperature, showing the enhanced
 166 cracking at elevated temperature. The higher variations in the C_2/C_1 ratio at lower temperatures was
 167 caused by greater relative fluctuations in the measured concentration of C_1 products.

168 The combined yield of propane and propylene was $\leq 10\%$ during the initial deactivation period
 169 (450-420 °C, 0-70 h). However, at the subsequent steady state period (380-400 °C, 70-170 h), this
 170 number was less than 1 %, and it remained low ($\leq 2\%$) during the remainder of the activity tests,
 171 indicating that active sites (probably acid sites) responsible for carbon-carbon bond formation had
 172 been deactivated.

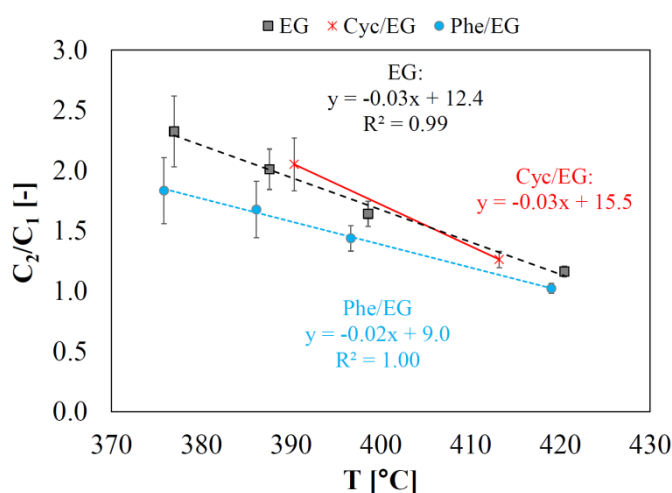
173
 174



175

176

177 **Figure 2.** Carbon based yields of: (a) Ethane; (b) Ethylene; (c) CO; (d) CH₄ from the conversion of
 178 ethylene glycol in experiments with pure ethylene glycol and mixtures of cyclohexanol/EG and
 179 phenol/EG. For experimental conditions, see Materials and Methods section 4.4, Table 6. Set point
 180 temperatures are shown (see also Figure 1).



181

182

183

184

185

186

Figure 3. Selectivity towards HDO compared to cracking expressed as the C_2/C_1 gaseous product ratio as a function of measured reaction temperature from the conversion of ethylene glycol in experiments with pure ethylene glycol and mixtures of cyclohexanol/EG and phenol/EG. For experimental conditions, see Materials and Methods section 4.4, Table 6. Data taken from the final 5 h of each operating temperature. Error bars show two standard deviations.

187

188

189

190

191

192

193

Calculated first order rate constants for each reaction temperature and fitted Arrhenius parameters based on these rate constants (for reactions 1a and 2a) are listed in Table 1, see section 4.5 for macro-kinetic model. Based on the evaluation of the Mears' criterion and the effectiveness factor [20] (Figure S4), it was concluded, that the experiments were conducted without significant external or internal diffusion limitations.

194

195

196

197

198

Table 1. First order rate constants as a function of reaction temperature, and apparent activation energies and rate constants at the mean temperature of 395 °C for the conversion of ethylene glycol (reactions 1a and 2a) as pure compound and in mixture with phenol and cyclohexanol. For experimental conditions, see Materials and Methods section 4.4, Table 6. For macro-kinetic model, see section 4.5.

Experiment	TOS [h]	T [°C]	$k'_{1a} \cdot 10^3$ [L/(min·g)]	$k'_{2a} \cdot 10^3$ [L/(min·g)]	$E_{a,1a}$ [kJ/mol]	$E_{a,2a}$ [kJ/mol]	$k'_{1a,mean} \cdot 10^3$ [L/(min·g)]	$k'_{2a,mean} \cdot 10^3$ [L/(min·g)]
EG	90-104	399	16.4	271				
	134-139	388	12.4	264	93.3	8.15	15.0	269
	165-170	377	9.41	258				
Phe/EG	99-104	397	14.2	250				
	134-139	386	10.8	235	95.9	22.1	13.6	248
	165-170	376	8.15	220				
Phe/EG-ReAct ¹	148-153	388	12.6	78.4	141	32.3	16.4	83.3
	173-178	377	8.19	71.1				
Cyc/EG	64-69	413	22.2	336	85.4	2.43	14.8	332
	85-90	390	13.3	331				

199 ¹ After catalyst reactivation, see Section 2.4.
200

201 The thermodynamic equilibrium of reactions 1a and 2a is fully shifted towards the product side
202 at the applied operating conditions (calculated with HSC Chemistry v. 9.4.1.). Incomplete conversion
203 of ethylene glycol was however obtained during steady state operation and ethylene and ethane were
204 formed at similar yields (Figure 1-Figure 2). Thus, the reaction mixture was far from equilibrium,
205 possibly partly due to the initial loss of hydrogenation activity. The hydrogenation of ethylene had a
206 low apparent activation energy of 2.4-32 kJ/mol and a rate constant, $k'_{2a,mean}$, which for the fresh
207 catalysts was 18-22 times larger than that of the initial dehydration and hydrogenation of oxygenates
208 into ethylene, $k'_{1a,mean}$. Although this fast hydrogenation of ethylene was probably affected by mass
209 transfer limitations, giving a low apparent activation energy, the trend in reactivity remains
210 unaffected.

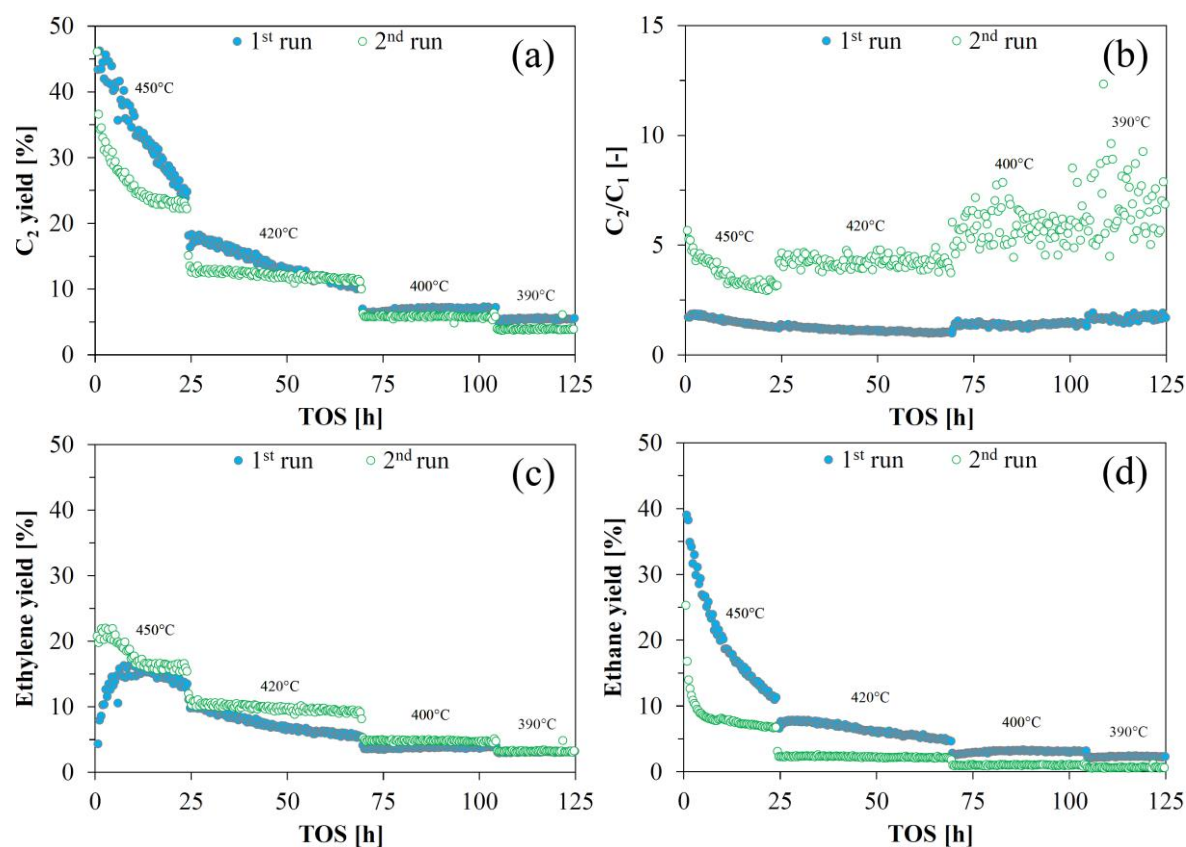
211 The kinetics of ethylene glycol HDO were rather similar for ethylene glycol as pure feed or in
212 the presence of phenol or cyclohexanol, especially for the first dehydration and hydrogenation step
213 where $k'_{1a,mean} = 14-16 \cdot 10^{-3}$ L/(min·g) and $E_{a,1a} = 85-96$ kJ/mol, suggesting that no inhibition of ethylene
214 glycol HDO from phenol or cyclohexanol occurred (Figure S5a). The hydrogenation of ethylene was
215 more affected by the presence of phenol or cyclohexanol (Figure S5b). Cyclohexanol seemed to have
216 a slight promoting effect, while phenol seemed to have a slight inhibiting effect. Phenol is expected
217 to adsorb strongly onto the support [21,22], which may block the accessibility to active edge sites
218 responsible for hydrogenation and deoxygenation (brim sites and vacancies)[23–25], and thereby
219 limit this activity. Cyclohexanol dehydration is suggested to occur over the acid sites of the support,
220 and it is possible that this occupation of acid sites has prevented coke formation, keeping
221 hydrogenation sites accessible.

222 The reactivated catalyst showed a decreased hydrogenation rate and a significantly higher
223 barrier for the initial ethylene glycol dehydration and hydrogenation, as $k'_{2a,mean}$ decreased from 248-
224 $332 \cdot 10^{-3}$ L/(min·g) to $83 \cdot 10^{-3}$ L/(min·g) and $E_{a,1a}$ increased from 85-96 kJ/mol to 141 kJ/mol (Table 1).
225 This may be due to changes in the active phase (see below).
226
227

228 2.4. Catalyst Reactivation

229 If HDO of biomass feedstocks occurs during pyrolysis (as in catalytic fast hydrolysis), the
230 operating temperature should not be increased markedly, as this would favor gas formation and limit
231 the oil yield [1]. This means that catalyst reactivation cannot be performed analogously to
232 conventional hydrotreating, in which catalyst activity can be maintained by continuously increasing
233 the reaction temperature until the end of run temperature (the upper limit allowed by the equipment)
234 is reached [26]. If HDO on the other hand is carried out downstream of a pyrolysis unit, it allows for
235 a greater flexibility in the choice of operating temperature, as this step is decoupled from the
236 pyrolysis.

237 At the end of a catalytic cycle in conventional hydrotreating it is possible to regenerate the spent
238 catalyst ex-situ by combustion of deposited coke and reload it into the reactor [27]. Such an ex-situ
239 regeneration could be particularly suitable for HDO catalysts, where deactivation is faster. To test
240 this, the catalyst tested for HDO of the phenol/ ethylene glycol mixture was reactivated in-situ in the
241 reactor setup. Deposited carbon was removed in an oxidation step (545 °C in 7.6 % O₂ in N₂, Figure
242 S9), which left the active sulfide phase in a partially oxidized state requiring a resulfidation step to
243 convert the resulting MoO_xS_y phase back into the active MoS₂ phase. The concentrations of NO_x
244 (negligible), CO, CO₂, O₂, and SO₂ were monitored using an Emerson NGA 2000 gas analyzer. The
245 carbon deposition on the catalyst was calculated based on the flow of N₂ and O₂ into the system and
246 the measured concentrations of oxidation products and O₂, giving a carbon deposition of 15.4 wt%.
247 After resulfidation, the catalytic activity was measured again (EG/Phe-ReAct, Figure 1 and Figure 4).
248



249

250

251

252

253

254

255

Figure 4. Carbon based (a) C_2 yield; (b) C_2/C_1 ratio; (c) Ethylene yield, and (d) Ethane yield for the first 125 h on stream, where the reaction temperature was the same. Based on ethylene glycol. 1st run (Phe/EG) and 2nd run (reactivated catalyst, Phe/EG-ReAct). For experimental conditions, see Materials and Methods section 4.4, Table 6. Set point temperatures are shown (see also Figure 1). For conversion, see Figure 1.

256

257

258

259

260

261

262

263

264

265

Overall, reactivation of the catalyst was possible, as the yield of deoxygenated C_2 species of the reactivated catalyst (2nd run) was similar to the yield of the fresh catalyst (1st run). However, the reactivated catalyst showed a different rate of deactivation (especially at < 50 h). After a period of around 50 hours with deactivation, the C_2 yields from the 1st and 2nd run were similar (Figure 4a). The reactivated catalyst showed a different product selectivity with less cracking (Figure 4b) and less hydrogenation (Figure 4c and d). Particularly the hydrogenation activity was markedly lower for the reactivated catalyst. The reactivated catalyst's poorer activity for ethylene glycol HDO was evidenced by the increase in activation energy for the initial dehydration/hydrogenation, $E_{a,1a}$, from 96 to 141 kJ/mol, and by the decrease in the rate constant for hydrogenation, $k'_{2a,mean}$, from $248 \cdot 10^{-3}$ to $83 \cdot 10^{-3}$ L/(min·g) (Table 1).

266

267

268

269

270

271

272

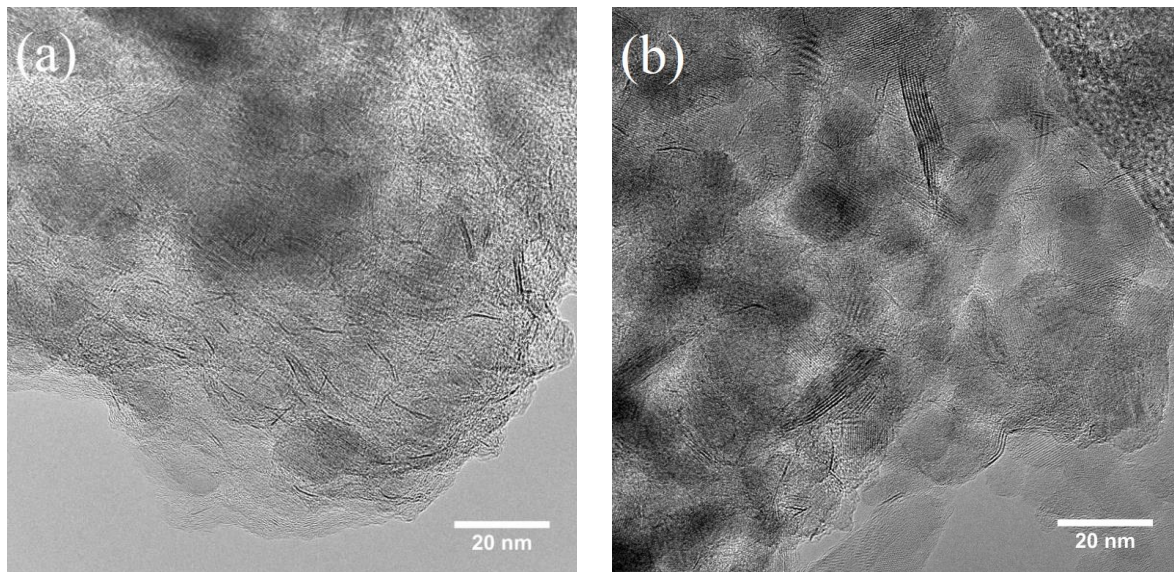
273

274

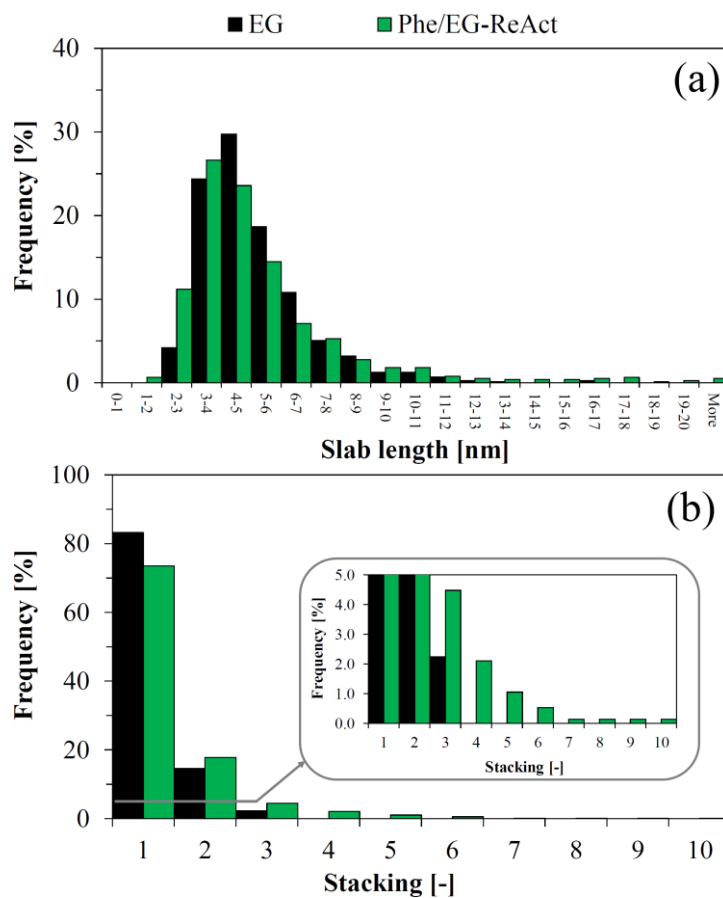
275

The size distribution of the active MoS_2 particles was obtained from analyses of TEM images (Figure 5 and Figure 6) of the spent catalysts from the experiment with pure ethylene glycol (EG) and with the phenol/ethylene glycol mixture including the reactivation step (Phe/EG-ReAct). The results indicate that some degree of sintering occurred during the reactivation process. In line with previous results [19], the observed average length (Figure 6a) and stacking (Figure 6b) for both spent catalysts were 5.1–5.3 nm and 1.2–1.4 nm, respectively. The majority of the observed sulfide particles in the spent catalyst samples were distributed as short monolayer slabs. The maximum degree of stacking was 3 for the non-activated catalyst, while several multilayer slabs with stacking degrees of 4–10 were observed in the reactivated spent sample (Figure 6b). These multilayer slabs were also longer than in the non-activated sample, as evidenced from the longer tail at >10 nm (Figure 6a).

276 As a result of the apparent sintering during catalyst reactivation, the concentration of active edge
 277 sites and brim sites (present at the top layer) has decreased, while the concentration of MoS₂ present
 278 in inactive bulk and basal plane positions has increased.
 279



280
 281 **Figure 5.** TEM images of the sulfided NiMo/MgAl₂O₄ catalyst after the experiments: (a) EG; (b)
 282 Phe/EG-ReAct.



286 **Figure 6.** Particle size distribution for spent catalysts from experiments EG and Phe/EG-ReAct: (a)
 287 Slab length; (b) Stacking. Based on > 700 slabs in > 40 TEM images for each sample.

288
289
290
291
292
293
294
295
296
297
298

The composition of the catalysts from the EG and Phe/EG-ReAct experiments is shown in Table 2. The molar Ni/Mo ratio was 0.3 (same as the fresh catalyst) in the non-reactivated spent catalyst from the EG experiment, whereas it had increased to 0.5 for the reactivated catalyst, indicating loss of Mo. MoO₃, which is formed during the initial oxidation stage of the regeneration, can be converted into volatile molybdenum hydroxy oxides in the presence of water [27,28]. Therefore, the oxidation conditions should be carefully controlled (low heating rate and high air flow) to limit the surface concentration of water formed during the combustion of carbonaceous materials from the catalyst. Especially the loss of brim sites along with the loss of Mo explains the loss of hydrogenation activity in the reactivated catalyst.

299

Table 2. Composition of the spent catalyst after long term experiments.

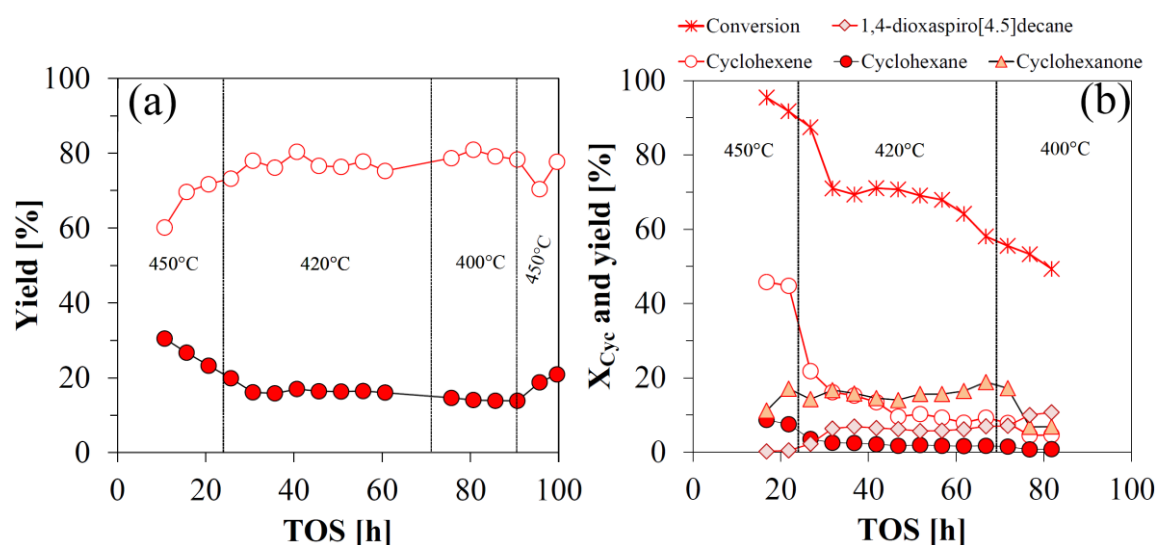
Experiment	TOS [h]	Mo [wt%]	Ni [wt%]	Ni/Mo [molar]	S [wt%]	C [wt%]	S/Mo [molar]
EG	221	2.55	0.46	0.29	1.71	18.8	2.00
Phe/EG-ReAct ¹	220(2 nd)	1.45	0.44	0.49	2.40	11.3	4.96

300
301
302
303
304
305
306

¹ After catalyst reactivation.

2.5. HDO of Cyclohexanol

HDO of cyclohexanol was performed on both the pure compound (Cyc) and as a cyclohexanol/ethylene glycol mixture (Cyc/EG), see Figure 7.



307
308
309
310
311
312

Figure 7. Carbon based product yields from the conversion of (a) Pure cyclohexanol (Cyc); (b) A cyclohexanol/ethylene glycol mixture (Cyc/EG). Based on cyclohexanol. For experimental conditions, see Materials and Methods section 4.4, Table 6. The conversion of cyclohexanol for the pure compound (a) was $\geq 99.5\%$ during the entire time on stream and is therefore not shown. Set point temperatures are shown.

313
314
315
316
317

Pure cyclohexanol was almost fully converted ($X_{Cyc} \geq 99.5\%$) during the entire duration of the activity test at 390–450 °C and a WHSV of 18 h⁻¹ (Figure 7a). Cyclohexene and cyclohexane were the dominant products, only trace amounts of cyclohexanone were detected (not shown). The yield of cyclohexene was 60–80 % and that of cyclohexane was 14–30 %. There was an initial decrease in the

318 yield of cyclohexane and increase in cyclohexene indicating some deactivation of hydrogenation
 319 activity as observed for the conversion of ethylene glycol. The first dehydration step of cyclohexanol
 320 into cyclohexene (reaction 1b) was very fast with a conversion above 90 % (Table 3). The measured
 321 rate may therefore be affected by mass transfer limitations.
 322

323 **Table 3.** First order rate constants as a function of reaction temperature, and apparent activation
 324 energies and rate constants at the mean temperature of 395 °C for the conversion of cyclohexanol
 325 (reactions 1b and 2b) as pure compound and in mixture with ethylene glycol. For experimental
 326 conditions, see Materials and Methods section 4.4, Table 6. For macro-kinetic model, see section 4.5.

Experimen t	TOS [h]	T [°C]	$k_{1b} \cdot 10^3$ [L/(min·g)]	$k'_{2b} \cdot 10^3$ [L/(min·g)]	$E_{a,1b}$ [kJ/mol]	$E_{a,2b}$ [kJ/mol]	$k_{1b,mean} \cdot 10^3$ [L/(min·g)]	$k'_{2b,mean} \cdot 10^3$ [L/(min·g)]
Cyc	53-63	413	$\geq 524^1$	55.1	-	43.3	-	45.2
	78-88	391	$\geq 524^1$	43.5	-	-	-	-
Cyc/EG	54-64	413	21.4	74.4	121	82.9	12.1	50.3
	74-84	390	10.3	44.9	-	-	-	-

327 ¹ Due to full conversion of cyclohexanol in this experiment, kinetic parameters were not fitted for
 328 reaction 1b. k_{1b} was calculated as $k_{1b} = -\frac{v}{W} \ln(1 - X_{1b})$, with $X_{1b} = (F_{CEN} + F_{CAN}) / F_{Cyc,feed}$, see
 329 section 4.5.

330
 331 In the presence of ethylene glycol (Figure 7b), >90 % conversion of cyclohexanol was initially
 332 obtained, decreasing to approximately 70 % after 30-65 h on stream, where an approximate steady
 333 state was obtained at 413 °C. As the temperature was decreased to the set point of 400 °C, the
 334 conversion continued to decrease reaching 49 % at 82 h on stream. Shortly after, setup issues forced
 335 termination of the experiment. The product composition from this experiment was comprised of
 336 cyclohexene, cyclohexane, cyclohexanone, and 1,4-dioxaspiro[4.5]decane (a ketal coupling product
 337 from cyclohexanone and ethylene glycol). The yield of HDO products were 4.5-16 % cyclohexene and
 338 0.7-2.5 % cyclohexane at TOS >30 h. The yields of by-products were significant: 5.7-11 % 1,4-
 339 dioxaspiro[4.5]decane, and 6.8-19 % cyclohexanone in the same time period.

340 As the conversion of cyclohexanol in the presence of ethylene glycol was performed at a four
 341 times higher residence time compared to the experiment with pure cyclohexanol (Table 6), these
 342 results show that ethylene glycol inhibited the conversion of cyclohexanol significantly. This was also
 343 reflected by the rate constants (Table 3). With ethylene glycol present in the feed, the rate constant,
 344 k_{1b} , decreased from $\geq 524 \cdot 10^{-3}$ L/(min·g) (independent on temperature) to $10-21 \cdot 10^{-3}$ L/(min·g), and
 345 there was a notable activation energy of 121 kJ/mol. This detrimental effect was explained by
 346 deactivation of acidic active sites by a competitive adsorption of ethylene glycol derived compounds
 347 (HDO intermediates and side products) as well as carbon deposition. The hydrogenation of
 348 cyclohexene was also affected by the presence of ethylene glycol, which caused the activation energy,
 349 $E_{a,2b}$, to double, while the rate constant remained more constant (at the reference temperature of 395
 350 °C). This could be caused by the competition for hydrogenation active sites.

351 As mentioned, the hydrogenation of ethylene (reaction 2a) was the fastest step in ethylene glycol
 352 HDO. For pure cyclohexanol, the initial dehydration to cyclohexene was the fastest step with k'_{2b}/k_{1b}
 353 ≤ 0.1 . This further indicates that the conversion of ethylene glycol and cyclohexanol takes place on
 354 different active sites. Full deoxygenation of cyclohexanol can occur on acid sites supplied by the
 355 support without interaction with the MoS₂ active phase, whereas ethylene glycol HDO depends on
 356 MoS₂ for hydrogenation of ethenol/acetaldehyde. The equilibrium of the reactions in Scheme 2 is fully
 357 shifted towards cyclohexane and benzene (Figure S6) at the applied reaction conditions. Cyclohexene
 358 is thermodynamically expected to occur in minute concentrations. Since benzene was not detected in

359 the liquid product, and cyclohexene was a dominant product, hydrogenation/dehydrogenation
360 activity was the limiting factor, possibly due to coking of Ni-MoS₂ active sites.

361 2.6. HDO of Phenol

362 Phenol, which was fed in a mixture with ethylene glycol, was not converted at the applied
363 conditions over the sulfided NiMo catalyst. The only products detected in low yields from phenol
364 were alkyl substituted phenols and coupling products (primarily 2-ethylphenol, 3-methylphenol, and
365 benzofuran), which were ascribed to the catalytic activity of the support acid sites [18]. These non-
366 deoxygenated coupling products were mainly formed during the first 30 h on stream at a total phenol
367 based carbon yield of up to 12 %. After 30 h, this yield was 0.4-3.7 %.

368 The lack of ring hydrogenation could explain the lack of phenol conversion. A NiMo catalyst
369 was chosen over a CoMo catalyst due to its known hydrogenation activity [29,30]. Ni-MoS₂ has been
370 reported to promote phenol HDO by aromatic ring hydrogenation (HYD) prior to breakage of the C-
371 O bond, whereas direct deoxygenation (DDO) can be performed with Co-MoS₂ [31–34].
372 Hydrogenation of the aromatic ring is however limited by thermodynamics (Figure S6-Figure S7)
373 and favored only at temperatures well below 300 °C. The temperature was therefore decreased to 280
374 °C (at 170-200 h) for the reactivated catalyst (Phe/EG-ReAct), based on the work of Mortensen et
375 al.[35], who reported ≈20-55 % phenol conversion over a Ni-MoS₂/ZrO₂ catalyst tested in the same
376 flow reactor setup for a TOS of 100 h at 280 °C, 100 bar, ≈283 vol ppm H₂S and a WHSV of 4.0 h⁻¹
377 of 50 g/L phenol in 1-octanol. No conversion of either ethylene glycol or phenol was however observed
378 at 280 °C.

379 Mechanistic effects may have contributed significantly to the lack of ring hydrogenation. It has
380 been proposed that HDO of phenolic species over Ni-MoS₂ requires a flat ring adsorption onto the
381 slab surface [33,36], which facilitates ring hydrogenation. If most active sites were occupied by
382 ethylene glycol, its derivatives, or coke, these species could sterically hinder flat ring adsorption of
383 phenol. Ryymin et al. [14] reported a slight suppression of methyl heptanoate HDO in the presence
384 of phenol at 250 °C and 75 bar using a commercial NiMo/Al₂O₃ catalyst in a batch reactor at reaction
385 times lower than 50 minutes. At the same time, they reported a notable inhibition of phenol HDO in
386 the presence of methyl heptanoate during the entire reaction time of ≈4.5-5 h, and suggested that the
387 inhibiting effect of the ester on phenol conversion was caused by a competition for active sites. This
388 is in line with the findings of Boscagli et al. [15], who showed that phenol HDO over Ni and Ru
389 catalysts was strongly inhibited in the presence of a light phase pyrolysis oil, mainly containing
390 cellulose derivatives. An additional possibility could be that the H₂S concentration, being a known
391 inhibitor in phenol HDO [32], was too high for phenol conversion in the current experiments.

392 393 2.7. HDO of Acetic Acid

394 The HDO of acetic acid was briefly tested at 450 °C with a feed of ≈0.06-0.13 mL/min acetic acid
395 corresponding to 1.0-2.3 mmol/min. After 2 h on stream, a coke plug developed in the reactor inlet
396 (above the catalyst bed), resulting in a pressure drop of 48 bar. This experiment clearly illustrated the
397 issues of heating reactive oxygenates, which others also have faced when using bio-oil for HDO
398 studies [37–39]. The short TOS resulted in the gas product yields summarized in Table 4, which
399 compares the yields with those from the conversion of pure ethylene glycol at similar conditions.

400 Acetic acid can undergo different reactions such as decarboxylation to form CH₄ and CO₂,
401 decarbonylation (of two acetic acid molecules) to form ethylene, CO, and water, and ketonization (of
402 two acetic acid molecules) to form acetone, CO₂, and water [40]. It is also possible that acetic acid can
403 be converted by HDO to acetaldehyde and water, allowing for similar reactions as for ethylene glycol.
404 The formation of acetone could be the reason for the high yield of propane and propylene formed
405 from acetic acid compared to ethylene glycol, which indicated the higher propensity for carboxylic
406 acids to polymerize. The ethane/ethylene ratio was higher (at ≈10) for acetic acid HDO compared to
407 ethylene glycol HDO (at ≈3), which could be due to differences in the mechanism for ethylene
408 formation. The higher yield of C₁ and coke from acetic acid HDO also indicated a higher degree of
409 cracking of acetic acid compared to ethylene glycol, which was partly caused by an up to 13 °C higher
410 reaction temperature (Figure S3).

411 **Table 4.** Gas product yields at TOS = 0-2 h for the conversion of ethylene glycol (EG) and acetic acid
 412 (AcOH) at 450 °C.

Experiment	CH ₄ [%]	CO [%]	CO ₂ [%]	Ethylene [%]	Ethane [%]	Propylene [%]	Propane [%]	Total carbon in gas phase [%]
EG	8-9	12-13	4-5	8-11	28-29	4-7	3	67-74
AcOH	17-21	17-20	7-8	2	21-24	8-11	9-11	83-93

413

414 2.8. Investigation of Catalyst Deactivation

415 In order to gain more insight into the deactivation routes, the spent catalysts were investigated
 416 in more detail. The composition of spent catalysts from several experiments is shown in Table 5 and
 417 it should be noted that the Ni/Mo ratio was constant at 0.3 indicating no loss of Mo or Ni (see also
 418 Table 2).

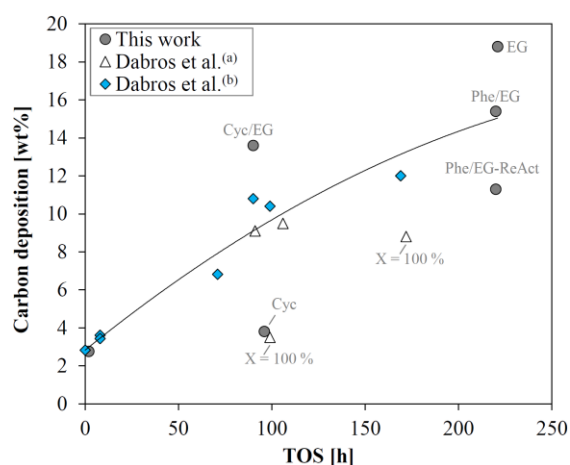
419

Table 5. Spent catalyst composition.

Experiment	TOS [h]	Mo [wt%]	Ni [wt%]	Ni/Mo [molar]	S [wt%]	C [wt%]	S/Mo [molar]
Phe/EG	220(1 st)	-	-	-	-	15.4	-
Cyc/EG	90	2.63	0.42	0.26	1.69	13.6	1.92
Cyc	96	2.96	0.51	0.28	2.18	3.81	2.51
AcOH	2	3.09	0.52	0.27	2.03	2.76	1.96

420

421 The amount of carbon deposited strongly depends on the time on stream (Figure 8). In line with
 422 previous reports [18,19], this is probably the main cause of deactivation. The severe carbon deposition
 423 is partly caused by a very high space velocity, which was chosen to facilitate steady state activity with
 424 a conversion below 100%. If the liquid hourly space velocity, LHSV, is decreased to obtain full
 425 conversion, the carbon deposition is expected to occur at a lower rate than observed here, based on
 426 the results from previous work [18]. The high amount of carbon (13.6 wt%) deposited on the catalyst
 427 from the experiment with the cyclohexanol/ethylene glycol mixture, was affected by the lack of N₂
 428 flushing at reaction temperature, as the experiment was terminated abruptly due to equipment
 429 malfunction.



430

431 **Figure 8.** Carbon deposition as a function of time on stream. From HDO tests performed at 380-450
 432 °C. Data from this work (Table 2 and Table 5, circles: text denotes experiment name), Dabros et al.^(a)

433 [18] (Table 3, triangles, X = 100 % denotes experiments with full conversion), and Dabros et al.^(b) [19]
434 (Table 2, diamonds).

435 TEM (Figure S8) indicated that the deposited carbon was present throughout the spent catalysts,
436 which is in agreement with previous findings [41]. The carbon appeared crystalline in agreement
437 with Raman spectroscopy data on similar catalysts [18]. The lattice distances were analyzed by
438 performing fast Fourier transforms of several crystalline areas in the TEM images of spent catalysts,
439 which showed the presence of the MgAl₂O₄ support, and indicated the presence of crystalline carbon
440 as well.

441 3. Discussion

442 This work clearly demonstrates the present and future challenges of bio-oil HDO. The different
443 reactivity and competitive adsorption of different oxygenate functionalities present in bio-oil make
444 catalytic HDO difficult as a one-step upgrading technique. While many HDO studies have
445 demonstrated promising reactivity of single model compounds over various catalyst systems, studies
446 on one-step upgrading of condensed bio-oil have revealed the challenge of dealing with complex
447 compound mixtures [37–39]. Model compound studies should therefore be used to provide valuable
448 insights by considering the interaction between several compounds with different functionalities, to
449 better understand the comprehensive network of reactions and interactions, such as competitive
450 inhibition and carbon deposition, which influence the activity and stability of the working catalyst
451 during HDO. Moreover, advanced preparation [42,43] and characterization [44] techniques continues
452 provide relevant contributions to the understanding and optimization of HDO over sulfided
453 catalysts.

454 More advanced techniques than one-step bio-oil upgrading are more promising. One option is
455 to perform the HDO step in-situ during fast pyrolysis as catalytic fast hydrolysis in a fluid bed
456 reactor [4,16,45–49]. In this way, reactive oxygenates can be upgraded immediately once they are
457 formed, and more stable compounds such as phenols, can be deoxygenated downstream.

458 Another option, which is in line with the idea of local fast pyrolysis and centralized bio-oil
459 upgrading, e.g. at a petrochemical refinery, is to perform multistage HDO of condensed bio-oil
460 [11,12,50–53]. Here, HDO is carried out in several stages at increasing temperature. In this way, the
461 most reactive cellulose derived compounds can be hydrogenated at low temperatures of 80–180 °C in
462 the first stage. The temperature is gradually increased in the subsequent stages to treat the more
463 refractory compounds, ending at a final temperature of 300–400 °C, which is suitable for
464 hydrocracking and deoxygenation of polyaromatics and heavy organic acids, which otherwise are
465 disturbed by the more reactive constituents [12]. The hydrogenation of carbonyls and polyols first
466 appears to be a good strategy, since no inhibition of ethylene glycol HDO by cyclohexanol or phenol
467 was observed, while strong inhibition of cyclohexanol and phenol HDO by ethylene glycol and rapid
468 coking of acetic acid was observed.

469 Catalyst deactivation is a critical challenge for all catalytic HDO techniques. Carbon deposition
470 should be minimized by operating at a high hydrogen pressure, a high hydrogen to bio-oil ratio and
471 a low bio-oil space velocity. Herein, it has been demonstrated that sulfide based catalysts can be
472 reactivated with appreciable activity and selectivity. As an important next step, we propose to
473 determine the true catalyst lifetime as well as whether the reactivation process is feasible at large
474 scale.

475 4. Materials and Methods

476 4.1. Catalyst Preparation and Characterization

477 A NiMo catalyst was prepared by sequential incipient wetness impregnation of 300–600 µm
478 sieve fraction of the MgAl₂O₄ support (prepared by calcination of Al₂O₃·MgO supplied by Sasol [19]).
479 The first impregnation was performed with an aqueous solution of ammonium heptamolybdate
480 hexahydrate (Fluka, ≥ 99.0 %). The second impregnation was performed with an aqueous solution of

481 nickel nitrate hexahydrate (Sigma-Aldrich, $\geq 97\%$). Each impregnation was followed by drying
 482 overnight at $110\text{ }^\circ\text{C}$. Finally, the catalyst was calcined in a flow of $2.5\text{ NL/min } 20\% \text{ O}_2$ in N_2 by heating
 483 with a ramp of $5\text{ }^\circ\text{C/min}$ to $500\text{ }^\circ\text{C}$ and holding for 3 h.

484 The fresh catalyst was characterized by inductively coupled plasma optical emission
 485 spectroscopy (ICP-OES) and N_2 -physisorption (BET). Spent catalyst samples were additionally
 486 characterized by transmission electron microscopy (TEM) and elemental C and S analysis. The latter
 487 was performed by combustion and infrared (IR) detection and quantification of the combustion
 488 products (CO_2 and SO_2). N_2 -physisorption was performed using a QuantaChrome Autosorb iQ₂ or
 489 Monosorb MS-21 gas sorption analyzer at liquid nitrogen temperature ($-196\text{ }^\circ\text{C}$). Catalyst outgassing
 490 was performed prior to N_2 -physisorption for 2 h at $350\text{ }^\circ\text{C}$ under vacuum. TEM was done using an
 491 aberration corrected FEI Titan 80-300 operated at 300 kV .

492 The calcined oxide phase catalyst contained $3.33\text{ wt}\%$ Mo and $0.66\text{ wt}\%$ Ni (molar Ni/Mo ratio =
 493 0.33). The specific surface BET area (SSA) was $77\text{ m}^2/\text{g}$.

494 4.2. Activity Testing

496 A high pressure fixed bed reactor setup (Figure S1) was used for the catalytic activity tests. The
 497 experimental procedure is described in the Electronic Supplementary Material (Figure S1- Figure S2).
 498 Catalyst activation was performed in the catalytic activity setup at close to atmospheric pressure in a
 499 flow of $10\text{-}12\text{ vol}\%$ H_2S . In activity tests, both the liquid model compound, or compound mixtures,
 500 and gas mixture (H_2 , N_2 , and $\text{H}_2\text{S}/\text{H}_2$) were fed to the reactor. The reactor effluent was separated into
 501 gas and liquid. The gas was analyzed online with gas chromatography (GC) using a thermal
 502 conductivity detector (TCD)). The liquid was collected and analyzed offline with GC using a flame
 503 ionization detector (FID) and mass spectrometry (MS), using effective carbon numbers for
 504 quantification [54]. Experiments were terminated by flushing the reactor with N_2 at ambient pressure
 505 and $\geq 400\text{ }^\circ\text{C}$ for 30 min to desorb any condensed species from the catalyst pores.

507 4.3. Calculations

508 The conversion, X , of model compound A was calculated based on the molar flow in, $F_{A,feed}$,
 509 and out, $F_{A,out}$, of the system:

$$510 \quad X_A = \frac{F_{A,feed} - F_{A,out}}{F_{A,feed}} \cdot 100\% \quad (1)$$

511 The carbon based yield, Y , of product i was calculated as:

$$512 \quad Y_i = \frac{F_i \cdot \nu_{C,i}}{F_{A,feed} \cdot \nu_{C,A}} \cdot 100\% \quad (2)$$

513 F_i is the molar flow rate of compound i , and $\nu_{C,i}$ is the number of carbon atoms in compound i . The
 514 product composition from each experiment showed that $\text{C}_1\text{-C}_3$ products were formed from ethylene
 515 glycol and not from cyclohexanol. Thus, in experiments with ethylene glycol, the yield of these
 516 compounds were calculated based on the ethylene glycol feed, and the yield ratio of desired HDO
 517 products (ethane and ethylene) to CO , CO_2 , and CH_4 was used as a measure of selectivity:
 518
 519
 520

$$521 \quad \frac{C_2}{C_1} = \frac{Y_{C_2H_6} + Y_{C_2H_4}}{Y_{CO} + Y_{CO_2} + Y_{CH_4}} \quad (3)$$

522 The yields of cyclic C_6 products from experiments with cyclohexanol were calculated on a
 523 cyclohexanol basis. In an experiment with both ethylene glycol and cyclohexanol in the feed, 1,4-
 524 dioxaspiro[4.5]decane ($\text{C}_8\text{H}_{14}\text{O}_2$) was formed. The yield of this compound was based on the

525 cyclohexanol feed by multiplication of the molar flow of $C_8H_{14}O_2$ with 6/8 to disregard the carbon
526 derived from ethylene glycol.

527 The model compound conversion as well as the yields of liquid products (e.g. cyclohexane and
528 cyclohexene) was generally subject to larger fluctuations than the yields of gaseous products. This
529 was caused by a longer stabilization time (from a low volumetric flow rate), a lower frequency in the
530 product analysis, and a less stable pressure reduction in the liquid product collection compared to
531 the gas product analysis (online GC-TCD measurements every 30 minutes). Typically, around 40 mL
532 liquid product was collected over the course of 5 hours, giving one data point, compared to around
533 10 GC-TCD measurements of the gaseous products within the same period of time.

534

535 4.4. Reaction Conditions

536 The conversion of acetic acid (AcOH, Sigma-Aldrich, $\geq 99.5\%$), ethylene glycol (EG, Sigma-
537 Aldrich, $\geq 99.8\%$), phenol (Phe, Sigma-Aldrich, $\geq 99\%$), and cyclohexanol (Cyc, Sigma-Aldrich, $\geq 99\%$)
538 in pure and mixed solutions was investigated using 0.5 g NiMo catalyst at 380-450 °C and 40 barg
539 with 27 bar H_2 and 550 vol ppm H_2S (total gas feed: 1550 NmL/min). The partial pressures of the
540 model compounds and products were low enough to keep them in the gas phase during reaction.

541 The conversion of pure ethylene glycol (experiment: EG) was compared with that of an ethylene
542 glycol feed containing either phenol (Phe/EG) or cyclohexanol (Cyc/EG). In these experiments, a
543 constant oxygen molar feed flow of 4.9 mmol/min was targeted (Table 6). An experiment with pure
544 cyclohexanol (Cyc) was performed to assess if cyclohexanol HDO had been affected by the presence
545 of ethylene glycol. In this experiment, the volumetric feed flow (0.16 mL/min) was used as design
546 parameter instead of the oxygen flow.

547

548 **Table 6.** Average model compound feed flow rates. Operating conditions: 27 bar H_2 , 550 vol ppm H_2S ,
549 40 barg total pressure (balance N_2). WHSV: Weight hourly space velocity in $g_{\text{model compound}}/(g_{\text{cat}} \cdot h)$. The
550 total flow of N_2 , H_2 , and H_2S was 69 mmol/min (1550 NmL/min).

Experiment / Parameter	EG	Phe/EG	Phe/EG-ReAct	Cyc/EG	Cyc
Molar flow rates [mmol/min]					
Ethylene glycol	2.5	2.2	2.2	2.2	0
Phenol	0	0.4	0.4	0	0
Cyclohexanol	0	0	0	0.4	1.5
Oxygen	4.9	4.9	4.9	4.8	1.5
Carbon	4.9	6.9	6.9	6.7	9.0
Total flow rate [mL/min]	0.14	0.16	0.16	0.16	0.16
Total WHSV [h⁻¹]	19	21	21	21	18

551

552 The activity tests were conducted for up to 220 h on stream. An initial accelerated deactivation
553 (at 420-450 °C) was performed (until 70 h) to avoid further loss of activity at 380-400 °C, which would
554 otherwise be observed [19]. The cyclohexanol/ethylene glycol experiment (Cyc/EG) was terminated
555 after 90 hours on stream due to equipment malfunction. For comparison, the pure cyclohexanol
556 experiment (Cyc) was also run for 90 hours on stream, followed by 10 hours at 450 °C before
557 experiment termination.

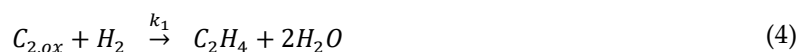
558

559 4.5. Macro-kinetic Model

560 Due to the lack of oxygenate quantification in the product gas and incomplete condensation of
561 acetaldehyde/ethanol and ethanol in the liquid products, the macro-kinetic model was set up with a
562 lumped $C_{2,ox}$ term covering ethylene glycol, ethenol, acetaldehyde, and ethanol as indicated in

563 Scheme 1. The kinetic model was based on the assumption of a constant hydrogen pressure (large
 564 excess) and first order kinetics for the remaining species. All species were assumed to be in the gas
 565 phase, and the total volumetric flow rate was assumed constant, which is a valid approximation for
 566 the highly diluted feed (see Table 6). The reactions included were the joint dehydration and
 567 hydrogenation of $C_{2,ox}$ into ethylene and the subsequent hydrogenation of ethylene into ethane:
 568

569 • Reaction 1a:



$$\Delta H = -47 \text{ kJ/mol}, \text{ at } 380\text{-}450 \text{ }^\circ\text{C for } C_{2,ox} = \text{EG} \quad (5)$$

570

571 • Reaction 2a:



$$\Delta H = -141 \text{ kJ/mol}, \text{ at } 380\text{-}450 \text{ }^\circ\text{C} \quad (7)$$

572

573 The reaction rate, r , of reaction 1a and 2a was set up using lumped rate constants k' and the
 574 concentration, C , of the lumped $C_{2,ox}$ compounds and ethylene (ETY):
 575

$$r_{1a} = k'_{1a} \cdot C_{C_{2,ox}} \quad (8)$$

$$r_{2a} = k'_{2a} \cdot C_{ETY} \quad (9)$$

576

577 The packed bed reactor model was used to set up molar flow balances for $C_{2,ox}$, ethylene, and
 578 ethane (ETA) based on reactions 1a and 2a:
 579

$$\frac{dF_{C_{2,ox}}}{dW} = -r_{1a} = -k'_{1a} \cdot C_{C_{2,ox}} \quad (10)$$

$$\frac{dF_{ETY}}{dW} = r_{1a} - r_{2a} = k'_{1a} \cdot C_{C_{2,ox}} - k'_{2a} \cdot C_{ETY} \quad (11)$$

$$\frac{dF_{ETA}}{dW} = r_{2a} = k'_{2a} \cdot C_{ETY} \quad (12)$$

580

581 W is the catalyst mass and F is the molar flow rate. The concentration was determined from the total
 582 gaseous volumetric flow rate, v , as $C_i = F_i / v$. The rate constants were parameterized at a mean
 583 temperature, T_{mean} , of 395 °C in order to decouple the activation energy and the pre-exponential factor:

$$k = k_{mean} \cdot \exp\left(\frac{-E_a}{R} \left(\frac{1}{T} - \frac{1}{T_{mean}}\right)\right) \quad (13)$$

584 T is the temperature in K, E_a is the apparent activation energy in kJ/mol and R is the gas constant
 585 ($8.314 \cdot 10^{-3}$ kJ/(K·mol)). The inlet molar flows of ethylene glycol ($F_{C_{2,ox,0}} = F_{C_{EG,0}}$), ethylene (zero), and
 586 ethane (zero), were used as initial conditions for the system of differential equations, which was
 587 solved, while k_{mean} and E_a were fitted.

588 The macro-kinetic model for HDO of cyclohexanol into cyclohexene (CEN) and cyclohexane
 589 (CAN) was derived similarly as to that for ethylene glycol as shown below. Hydrogen is not a reactant
 590 in reaction 1b, but in reaction 2b it is included in the lumped rate constant, k'_{2b} , with the assumption
 591 of being present in large excess:

592

$$\frac{dF_{Cyc}}{dW} = -r_{1b} = -k_{1b} \cdot C_{Cyc} \quad (14)$$

$$\frac{dF_{CEN}}{dW} = r_{1b} - r_{2b} = k_{1b} \cdot C_{Cyc} - k'_{2b} \cdot C_{CEN} \quad (15)$$

$$\frac{dF_{CAN}}{dW} = r_{2b} = k'_{2b} \cdot C_{CEN} \quad (16)$$

593

594

595

596

Only steady state data at each temperature was used, and for each steady state, the data used was the average from the final 5 hours at the given steady state.

597

5. Conclusions

598

599

600

601

602

603

604

605

606

The HDO of different biomass derived model compounds was investigated at 380–450 °C, 27 bar H₂, and 550 vol ppm H₂S over a Ni-MoS₂/MgAl₂O₄ catalyst. The results demonstrate a pronounced different reactivity of the compounds in HDO, ranging from the highly reactive acetic acid, which rapidly coked up the reactor inlet, to phenol, which only underwent limited alkyl substitution reactions with low yields. In addition, the HDO reactions were strongly influenced by the presence of several compounds. Ethylene glycol was readily converted in the presence and absence of cyclohexanol and phenol without significant influence on the macro-kinetic parameters. However, cyclohexanol deoxygenation was strongly inhibited by ethylene glycol, due to competitive adsorption and carbon deposition on acid sites.

607

608

609

610

611

612

613

614

615

This study proves the necessity of investigating HDO of mixed cellulose and lignin derived model compounds in the attempt to understand the reactions occurring during upgrading of real biomass based feeds. The results indicate that immediate stabilization of reactive cellulose fragments, i.e. before condensation, may be beneficial in order to reduce catalyst coking and avoid inhibition of the HDO of less reactive oxygenates. Alternatively, pyrolysis oil upgrading could be performed in several steps – first removing the most reactive compounds, then the less reactive ones. The industrial potential of sulfide based catalysts for HDO was strengthened by the regenerability of the applied Ni-MoS₂ catalyst. Deposited carbon could be removed from a spent catalyst by oxidation and resulfidation.

616

617

618

Future steps in the assessment of the commercial viability of the Ni-MoS₂/MgAl₂O₄HDO catalyst should focus on bridging the gap between more complex model compound mixtures and real feeds as well as assessing the industrial catalyst lifetime and optimizing the reactivation conditions.

619

620

621

622

623

624

625

626

627

628

629

630

631

632

633

634

635

636

Supplementary Materials: The following are available online at www.mdpi.com/xxx/s1, Figure S1: Simplified process diagram of the continuous flow fixed bed reactor setup. P: pump. MFC: Mass flow controller. PIC: Pressure indicator and controller. S1: Separator. dP: Differential pressure cell. C1: Condenser. V1-V8: Magnetic valves, Figure S2: Schematic drawing of reactor design including pressure shell, internal reactor, and thermo pocket. The gas and liquid inlets are shown. The insert to the right shows the gas and liquid feed flow paths at the internal reactor tube inlet, Figure S3: Initial temperature profiles. In the experiment with acetic acid (AcOH), the acetic acid feed was stopped at TOS ≈ 2.2 h, Figure S4: Effectiveness factor estimated for the fastest reaction in the conversion of ethylene glycol (dashed line) and cyclohexanol (solid line) as a function of catalyst particle radius. The actual particle radius used in HDO activity tests (150–300 μm) is shaded, Figure S5: Arrhenius plots for the rate constants presented in the main manuscript (Table 1). (a) k'1a: Initial dehydration and hydrogenation of C_{2,ox} into ethylene. (b) k'2a: Hydrogenation of ethylene into ethane, Figure S6: Equilibrium composition during cyclohexanol HDO calculated with HSC Chemistry v. 9.4.1. Feed composition: 2.1 kmol cyclohexanol, 66.1 kmol H₂, and 31.8 kmol N₂. Products included: H₂O, cyclohexane, cyclohexene, and benzene. The concentration of cyclohexene is multiplied with 100 for visualization, Figure S7: Equilibrium composition during phenol HDO calculated with HSC Chemistry v. 9.4.1. Feed composition: 0.55 kmol phenol, 65 kmol H₂, and 31.2 kmol N₂. Products included: H₂O, cyclohexane, benzene, Figure S8: TEM image of spent catalyst from the experiment: EG, Figure S9: Off-gas concentration profiles and temperature profile from carbon burnoff from the spent catalyst after experiment Phe/EG (before Phe/EG-ReAct). Performed in-situ with 1 NL/min 7.6 %O₂ in N₂.

637 **Author Contributions:** Conceptualization, Martin Høj, Jostein Gabrielsen, Jan-Dierk Grunwaldt and Anker
638 Degn Jensen; Funding acquisition, Martin Høj, Jostein Gabrielsen, Jan-Dierk Grunwaldt and Anker Degn Jensen;
639 Investigation, Trine Marie Hartmann Dabros, Mads Lysgaard Andersen, Simon Brædder Lindahl and Thomas
640 Willum Hansen; Project administration, Martin Høj, Jostein Gabrielsen, Jan-Dierk Grunwaldt and Anker Degn
641 Jensen; Supervision, Martin Høj, Jostein Gabrielsen, Jan-Dierk Grunwaldt and Anker Degn Jensen; Writing –
642 original draft, Trine Marie Hartmann Dabros; Writing – review & editing, Trine Marie Hartmann Dabros, Martin
643 Høj, Jan-Dierk Grunwaldt and Anker Degn Jensen.

644 **Funding:** This research was funded by The Danish Council for Strategic Research (now: Innovation Fund
645 Denmark) project 1305-00015B, The Programme Commission on Sustainable Energy and Environment.

646 **Acknowledgments:** This work is part of the H₂CAP (hydrogen assisted catalytic pyrolysis for green fuels) project
647 conducted at The Department of Chemical and Biochemical Engineering at DTU, Denmark. The technicians and
648 workshop at DTU Chemical and Biochemical Engineering are acknowledged for the construction and
649 maintenance of the experimental setup.

650 **Conflicts of Interest:** The authors declare no conflict of interest. The sponsors or other funding bodies had no
651 role in the design, execution, interpretation, or writing of the study.

652 References

- 653 1. Bridgwater, A.V. Review of fast pyrolysis of biomass and product upgrading. *Biomass and*
654 *Bioenergy* **2012**, *38*, 68–94.
- 655 2. Stummann, M.Z.; Høj, M.; Hansen, A.B.; Davidsen, B.; Wiwel, P.; Gabrielsen, J.; Jensen, P.A.;
656 Jensen, A.D. New insights into the effect of pressure on catalytic hydrolysis of biomass.
657 *Fuel Process. Technol.* **2019**, *193*, 392–403.
- 658 3. Venderbosch, R.H. A critical view on catalytic pyrolysis of biomass. *ChemSusChem* **2015**, *8*,
659 1306–1316.
- 660 4. Resende, F.L.P. Recent advances on fast hydrolysis of biomass. *Catal. Today* **2016**, *269*,
661 148–155.
- 662 5. Furimsky, E. Catalytic hydrodeoxygenation. *Appl. Catal. A Gen.* **2000**, *199*, 147–190.
- 663 6. Dabros, T.M.H.; Stummann, M.Z.; Høj, M.; Jensen, P.A.; Grunwaldt, J.-D.; Gabrielsen, J.;
664 Mortensen, P.M.; Jensen, A.D. Transportation fuels from biomass fast pyrolysis, catalytic
665 hydrodeoxygenation, and catalytic fast hydrolysis. *Prog. Energy Combust. Sci.* **2018**, *68*,
666 268–309.
- 667 7. Wang, H.; Male, J.; Wang, Y. Recent advances in hydrotreating of pyrolysis bio-oil and its
668 oxygen-containing model compounds. *ACS Catal.* **2013**, *3*, 1047–1070.
- 669 8. Azeez, A.M.; Meier, D.; Odermatt, J.; Willner, T. Fast pyrolysis of African and European
670 lignocellulosic biomasses using Py-GC/MS and fluidized bed reactor. *Energy & Fuels* **2010**, *24*,
671 2078–2085.
- 672 9. Mante, O.D.; Babu, S.P.; Amidon, T.E. A comprehensive study on relating cell-wall
673 components of lignocellulosic biomass to oxygenated species formed during pyrolysis. *J. Anal.*
674 *Appl. Pyrolysis* **2014**, *108*, 56–67.

- 675 10. Oasmaa, A.; Kuoppala, E.; Solantausta, Y. Fast pyrolysis of forestry residue. 2.
676 Physicochemical composition of product liquid. *Energy & Fuels* **2003**, *17*, 433–443.
- 677 11. Elliott, D.C. Historical developments in hydroprocessing bio-oils. *Energy & Fuels* **2007**, *21*,
678 1792–1815.
- 679 12. Yin, W.; Kloekhorst, A.; Venderbosch, R.H.; Bykova, M. V.; Khromova, S.A.; Yakovlev, V.A.;
680 Heeres, H.J. Catalytic hydrotreatment of fast pyrolysis liquids in batch and continuous set-
681 ups using a bimetallic Ni–Cu catalyst with a high metal content. *Catal. Sci. Technol.* **2016**, *6*,
682 5899–5915.
- 683 13. Dwiatmoko, A.A.; Lee, S.; Ham, H.C.; Choi, J.-W.; Suh, D.J.; Ha, J.-M. Effects of carbohydrates
684 on the hydrodeoxygenation of lignin- derived phenolic compounds. *ACS Catal.* **2015**, *5*, 433–
685 437.
- 686 14. Ryymin, E.-M.; Honkela, M.L.; Viljava, T.-R.; Krause, A.O.I. Competitive reactions and
687 mechanisms in the simultaneous HDO of phenol and methyl heptanoate over sulphided
688 NiMo/ γ -Al₂O₃. *Appl. Catal. A Gen.* **2010**, *389*, 114–121.
- 689 15. Boscagli, C.; Raffelt, K.; Grunwaldt, J.-D. Reactivity of platform molecules in pyrolysis oil and
690 in water during hydrotreatment over nickel and ruthenium catalysts. *Biomass and Bioenergy*
691 **2017**, *106*, 63–73.
- 692 16. Stummann, M.Z.; Høj, M.; Schandel, C.B.; Hansen, A.B.; Wiwel, P.; Gabrielsen, J.; Jensen, P.A.;
693 Jensen, A.D. Hydrogen assisted catalytic biomass pyrolysis. Effect of temperature and
694 pressure. *Biomass and Bioenergy* **2018**, *115*, 97–107.
- 695 17. Trinh, T.N.; Jensen, P.A.; Dam-Johansen, K.; Knudsen, N.O.; Sørensen, H.R.; Hvilsted, S.
696 Comparison of lignin, macroalgae, wood, and straw fast pyrolysis. *Energy & Fuels* **2013**, *27*,
697 1399–1409.
- 698 18. Dabros, T.M.H.; Kramer, H.; Høj, M.; Sprenger, P.; Gabrielsen, J.; Grunwaldt, J.-D.; Jensen,
699 A.D. The influence of active phase loading on the hydrodeoxygenation (HDO) of ethylene
700 glycol over promoted MoS₂/MgAl₂O₄ catalysts. *Top. Catal.* **2019**,
701 <https://doi.org/10.1007/s11244-019-01169-y>.
- 702 19. Dabros, T.M.H.; Gaur, A.; Pintos, D.G.; Sprenger, P.; Høj, M.; Hansen, T.W.; Studt, F.;
703 Gabrielsen, J.; Grunwaldt, J.D.; Jensen, A.D. Influence of H₂O and H₂S on the composition,
704 activity, and stability of sulfided Mo, CoMo, and NiMo supported on MgAl₂O₄ for
705 hydrodeoxygenation of ethylene glycol. *Appl. Catal. A Gen.* **2018**, *551*, 106–121.
- 706 20. Fogler, S.H. *Elements of Chemical Reaction Engineering*; 4th ed.; Pearson Education International,
707 Prentice Hall: Westford, Massachusetts, 2010;
- 708 21. Popov, A.; Kondratieva, E.; Goupil, J.M.; Mariey, L.; Bazin, P.; Gilson, J.-P.; Travert, A.; Mauge,
709 F. Bio-oils hydrodeoxygenation: Adsorption of phenolic molecules on oxidic catalyst

- 710 supports. *J. Phys. Chem. C* **2010**, *114*, 15661–15670.
- 711 22. Popov, A.; Kondratieva, E.; Mariey, L.; Goupil, J.M.; El Fallah, J.; Gilson, J.-P.; Travert, A.;
712 Maugé, F. Bio-oil hydrodeoxygenation: Adsorption of phenolic compounds on sulfided
713 (Co)Mo catalysts. *J. Catal.* **2013**, *297*, 176–186.
- 714 23. Bruix, A.; Füchtbauer, H.G.; Tuxen, A.K.; Walton, A.S.; Andersen, M.; Porsgaard, S.;
715 Besenbacher, F.; Hammer, B.; Lauritsen, J. V. In situ detection of active edge sites in single-
716 layer MoS₂ catalysts. *ACS Nano* **2015**, *9*, 9322–9330.
- 717 24. Grønborg, S.S.; Šarić, M.; Moses, P.G.; Rossmeisl, J.; Lauritsen, J. V. Atomic scale analysis of
718 sterical effects in the adsorption of 4,6-dimethyldibenzothiophene on a CoMoS hydrotreating
719 catalyst. *J. Catal.* **2016**, *344*, 121–128.
- 720 25. Šarić, M.; Rossmeisl, J.; Moses, P.G. Modeling the adsorption of sulfur containing molecules
721 and their hydrodesulfurization intermediates on the Co-promoted MoS₂ catalyst by DFT. *J.*
722 *Catal.* **2018**, *358*, 131–140.
- 723 26. Furimsky, E.; Massoth, F.E. Deactivation of hydroprocessing catalysts. *Catal. Today* **1999**, *52*,
724 381–495.
- 725 27. Dufresne, P. Hydroprocessing catalysts regeneration and recycling. *Appl. Catal. A Gen.* **2007**,
726 *322*, 67–75.
- 727 28. Smolik, G.R.; Petti, D.A.; Schuetz, S.T. *Oxidation, volatilization, and redistribution of molybdenum*
728 *from TZM alloy in air. INEEL/EXT-99-01353*; Idaho National Engineering and Environmental
729 Laboratory, 2000;
- 730 29. Schachtl, E.; Yoo, J.S.; Gutiérrez, O.Y.; Studt, F.; Lercher, J.A. Impact of Ni promotion on the
731 hydrogenation pathways of phenanthrene on MoS₂/γ-Al₂O₃. *J. Catal.* **2017**, *352*, 171–181.
- 732 30. Prins, R. Chapter 13.2: Hydrotreating. In *Handbook of Heterogeneous Catalysis*; Wiley-VCH
733 Verlag GmbH & Co. KGaA: E-book, 2008; pp. 2695–2718.
- 734 31. Bui, V.N.; Laurenti, D.; Afanasiev, P.; Geantet, C. Hydrodeoxygenation of guaiacol with CoMo
735 catalysts. Part I: Promoting effect of cobalt on HDO selectivity and activity. *Appl. Catal. B*
736 *Environ.* **2011**, *101*, 239–245.
- 737 32. Şenol, O.İ.; Ryymin, E.-M.; Viljava, T.-R.; Krause, A.O.I. Effect of hydrogen sulphide on the
738 hydrodeoxygenation of aromatic and aliphatic oxygenates on sulphided catalysts. *J. Mol.*
739 *Catal. A Chem.* **2007**, *277*, 107–112.
- 740 33. Bouvier, C.; Romero, Y.; Richard, F.; Brunet, S. Effect of H₂S and CO on the transformation of
741 2-ethylphenol as a model compound of bio-crude over sulfided Mo-based catalysts:
742 propositions of promoted active sites for deoxygenation pathways based on an experimental
743 study. *Green Chem.* **2011**, *13*, 2441–2451.

- 744 34. Gonçalves, V.O.O.; Brunet, S.; Richard, F. Hydrodeoxygenation of cresols over Mo/Al₂O₃ and
745 CoMo/Al₂O₃ sulfided catalysts. *Catal. Letters* **2016**, *146*, 1562–1573.
- 746 35. Mortensen, P.M.; Gardini, D.; Damsgaard, C.D.; Grunwaldt, J.-D.; Jensen, P.A.; Wagner, J.B.;
747 Jensen, A.D. Deactivation of Ni-MoS₂ by bio-oil impurities during hydrodeoxygenation of
748 phenol and octanol. *Appl. Catal. A Gen.* **2016**, *523*, 159–170.
- 749 36. Romero, Y.; Richard, F.; Brunet, S. Hydrodeoxygenation of 2-ethylphenol as a model
750 compound of bio-crude over sulfided Mo-based catalysts: Promoting effect and reaction
751 mechanism. *Appl. Catal. B Environ.* **2010**, *98*, 213–223.
- 752 37. Baldauf, W.; Balfanz, U.; Rupp, M. Upgrading of flash pyrolysis oil and utilization in
753 refineries. *Biomass and Bioenergy* **1994**, *7*, 237–244.
- 754 38. Elliott, D.C.; Hart, T.R.; Neuenschwander, G.G.; Rotness, L.J.; Zacher, A.H. Catalytic
755 hydroprocessing of biomass fast pyrolysis bio-oil to produce hydrocarbon products. *Environ.*
756 *Prog. Sustain. Energy* **2009**, *28*, 441–449.
- 757 39. Cordero-Lanzac, T.; Palos, R.; Arandes, J.M.; Castaño, P.; Rodríguez-Mirasol, J.; Cordero, T.;
758 Bilbao, J. Stability of an acid activated carbon based bifunctional catalyst for the raw bio-oil
759 hydrodeoxygenation. *Appl. Catal. B Environ.* **2017**, *203*, 389–399.
- 760 40. Lemonidou, A.A.; Kechagiopoulos, P.; Heracleous, E.; Voutetakis, S. Chapter 14: Steam
761 reforming of bio-oils to hydrogen. In *The role of catalysis for the sustainable production of bio-fuels*
762 *and bio-chemicals*; Triantafyllidis, K., Lappas, A., Stöcker, M., Eds.; Elsevier, 2013; pp. 467–493.
- 763 41. van Doorn, J.; Moulijn, J.A.; Djéga-Mariadassou, G. High-resolution electron microscopy of
764 spent Ni-Mo/Al₂O₃ hydrotreating catalysts. *Appl. Catal.* **1990**, *63*, 77–90.
- 765 42. Liu, G.; Robertson, A.W.; Li, M.M.-J.; Kuo, W.C.H.; Darby, M.T.; Muhieddine, M.H.; Lin, Y.-
766 C.; Suenaga, K.; Stamatakis, M.; Warner, J.H.; et al. MoS₂ monolayer catalyst doped with
767 isolated Co atoms for the hydrodeoxygenation reaction. *Nat. Chem.* **2017**, *9*, 810–816.
- 768 43. Song, W.; Nie, T.; Lai, W.; Yang, W.; Jiang, X. Tailoring the morphology of Co-doped MoS₂ for
769 enhanced hydrodeoxygenation performance of p-cresol. *CrystEngComm* **2018**, *20*, 4069–4074.
- 770 44. Gaur, A.; Dabros, T.M.H.; Høj, M.; Boubnov, A.; Prüssmann, T.; Jelic, J.; Studt, F.; Jensen, A.D.;
771 Grunwaldt, J.-D. Probing the active sites of MoS₂ based hydrotreating catalysts using
772 modulation excitation spectroscopy. *ACS Catal.* **2019**, *9*, 2568–2579.
- 773 45. Marker, T.L.; Felix, L.G.; Linck, M.B.; Roberts, M.J. Integrated hydrolysis and
774 hydroconversion (IH²) for the direct production of gasoline and diesel fuels or blending
775 components from biomass, part 1: Proof of principle testing. *Environ. Prog. Sustain. Energy*
776 **2012**, *31*, 191–199.
- 777 46. Marker, T.L.; Felix, L.G.; Linck, M.B.; Roberts, M.J.; Ortiz-toral, P.; Wangerow, J. Integrated
778 hydrolysis and hydroconversion (IH²) for the direct production of gasoline and diesel

- 779 fuels or blending components from biomass , part 2: Continuous testing. *Environ. Prog.*
780 *Sustain. Energy* **2014**, *33*, 762–768.
- 781 47. Stummann, M.Z.; Hansen, A.B.; Hansen, L.P.; Davidsen, B.; Rasmussen, S.B.; Wiwel, P.;
782 Gabrielsen, J.; Jensen, P.A.; Jensen, A.D.; Høj, M. Catalytic hydropyrolysis of biomass using
783 molybdenum sulfide based catalyst. Effect of promoters. *Energy & Fuels* **2019**, *33*, 1302–1313.
- 784 48. Stummann, M.Z.; Høj, M.; Davidsen, B.; Hansen, A.B.; Hansen, L.P.; Wiwel, P.; Schandel, C.B.;
785 Gabrielsen, J.; Jensen, P.A.; Jensen, A.D. Effect of the catalyst in fluid bed catalytic
786 hydropyrolysis. *Catal. Today* **2019**, *In press*.
- 787 49. Dayton, D.C.; Hlebak, J.; Carpenter, J.R.; Wang, K.; Mante, O.D.; Peters, J.E. Biomass
788 hydropyrolysis in a fluidized bed reactor. *Energy & Fuels* **2016**, *30*, 4879–4887.
- 789 50. Routray, K.; Barnett, K.J.; Huber, G.W. Hydrodeoxygenation of pyrolysis oils. *Energy Technol.*
790 **2017**, *5*, 80–93.
- 791 51. Elliott, D.C.; Neuenschwander, G.G.; Hart, T.R. Hydroprocessing bio-oil and products
792 separation for coke production. *ACS Sustain. Chem. Eng.* **2013**, *1*, 389–392.
- 793 52. Zacher, A.H.; Elliott, D.C.; Olarte, M. V.; Santosa, D.M.; Preto, F.; Iisa, K. Pyrolysis of woody
794 residue feedstocks: Upgrading of bio-oils from mountain-pine-beetle-killed trees and hog
795 fuel. *Energy & Fuels* **2014**, *28*, 7510–7516.
- 796 53. Olarte, M. V.; Padmaperuma, A.B.; Ferrell III, J.R.; Christensen, E.D.; Hallen, R.T.; Lucke, R.B.;
797 Burton, S.D.; Lemmon, T.L.; Swita, M.S.; Fioroni, G.; et al. Characterization of upgraded fast
798 pyrolysis oak oil distillate fractions from sulfided and non-sulfided catalytic hydrotreating.
799 *Fuel* **2017**, *202*, 620–630.
- 800 54. Schofield, K. The enigmatic mechanism of the flame ionization detector: Its overlooked
801 implications for fossil fuel combustion modeling. *Prog. Energy Combust. Sci.* **2008**, *34*, 330–350.

802



© 2019 by the authors. Submitted for possible open access publication under the terms and conditions of the Creative Commons Attribution (CC BY) license (<http://creativecommons.org/licenses/by/4.0/>).

803